Title
Limiting Current in Nanostructured Block Copolymer Electrolytes

Journal
Macromolecules, 54(9)

ISSN
0024-9297

Authors
Maslyn, Jacqueline A
Frenck, Louise
Veeraraghavan, Vijay D
et al.

Publication Date
2021-05-11

DOI
10.1021/acs.macromol.1c00425

Peer reviewed

Limiting Current in Nanostructured Block Copolymer Electrolytes

*Jacqueline A. Maslyn [a, b], Louise Frenck [a], Vijay D. Veeraraghavan [a], Alexander Müller [c], Alec S. Ho [a], Nandan Marwaha [a], Whitney S. Loo [a], Dilworth Y. Parkinson [d], Andrew M. Minor [c, e], Nitash P. Balsara [a, b, f, *]*

[a] Department of Chemical and Biomolecular Engineering, University of California, Berkeley, California 94720, USA

[b] Materials Sciences Division, Lawrence Berkeley National Laboratory, Berkeley, California, 94720, USA

[c] National Center for Electron Microscopy, Lawrence Berkeley National Laboratory, Berkeley, California 94720, USA

[d] Advanced Light Source, Lawrence Berkeley National Laboratory, Berkeley, California 94720, USA

[e] Department of Materials Science and Engineering, University of California, Berkeley, California 94720, USA

[f] Energy Technologies Area, Lawrence Berkeley National Laboratory, Berkeley, California 94720, USA

* Corresponding author. E-mail: nbalsara@berkeley.edu, Phone: 1-510-642-8973.

KEYWORDS.

Limiting current, polymer electrolytes, lithium ion transport properties, concentrated solution theory, rechargeable batteries

TOC

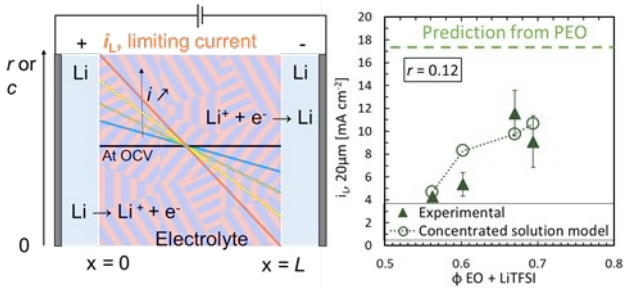

ABSTRACT

Next-generation electrolytes for lithium batteries must be able to conduct ions at sufficiently high current densities, yet this regime is rarely studied directly. The limiting current density of an electrolyte quantifies the highest possible rate of ion transport under an applied dc potential. Herein, we report on the limiting current density in twelve nanostructured polystyrene-*block*-poly(ethylene oxide) (PS-*b*-PEO, or SEO) copolymer electrolytes. We find that the limiting current at a given salt concentration increases systematically with increasing volume fraction of the PEO block (φ_{EO}). In contrast, effective medium theory, commonly used to analyze

conductivity in block copolymer electrolytes, predicts that limiting current is independent of φ_{EO}. To resolve this conundrum, the ionic conductivity, the mutual diffusion coefficient of the salt, and the steady-state current fraction of the block copolymer electrolytes were measured. These measurements enable predictions of limiting current with no adjustable parameters using concentrated solution theory. We found quantitative agreement between experimentally measured limiting current densities and predictions based on concentrated solution theory. This work sheds light on how to reliably measure and predict limiting current density in composite electrolytes.

INTRODUCTION

Smaller, lighter, more powerful batteries will help drive the next generation of mobile technologies with energy from renewable sources. Battery chemistries incorporating a lithium metal anode offer high theoretical specific energies and energy densities, but a compatible electrolyte with adequate performance has not yet been developed, despite considerable effort.[1–5] A suitable electrolyte must promote reversible lithium metal electrodeposition and stripping, and also conduct ions at a sufficiently high rate. Nanostructured rigid electrolytes have shown promise for this purpose: such materials contain conducting domains for ion transport and rigid domains to promote stable lithium deposition.[6,7] The ion transport properties of such composite materials are not easily predicted solely from ion transport properties of the conducting domain alone.

They are several key transport performance metrics for the evaluation of electrolytes wherein the charge carriers are in the form of added salt ions. We refer to a particular electrolyte as a salt-solvent combination of a specific concentration. An important one is the current-voltage

relationship in an electrolyte at steady-state; salt concentration gradients are induced when dc current flows through the electrolyte.[8–11] Another metric is the limiting current density, which is defined as the maximum steady-state current density achievable through a particular electrolyte.[12–15] At the limiting current density, the salt concentration at the cathode is identically zero.[16,17] Thus, when the applied current density exceeds the limiting current density, the Li^+ redox reaction cannot occur at this electrode at steady-state. Instead, the electrons at the electrode participate in irreversible reactions that lead to degradation of the electrolyte.

While the importance of limiting current density is well established in the literature, it is rarely measured in electrolytes with lithium ions.[18–22] One polymer electrolyte system that has been extensively studied is mixtures of poly(ethylene oxide) (PEO) and lithium bis(trifluoromethanesulfonyl)imide (LiTFSI).[23] Herein, we report on the limiting current density in twelve nanostructured polystyrene-*block*-poly(ethylene oxide) (PS-*b*-PEO, or SEO) copolymer electrolytes, obtained by combining four SEO block copolymers and three LiTFSI concentrations. These electrolytes self-assemble into lamellar morphologies, with alternating layers of ion-conducting PEO domains and mechanically reinforcing PS domains. The salt is preferentially located in the PEO-rich lamellae. Neutron spin echo measurements have shown that segmental motion of the ion-containing domains in block copolymer electrolytes is similar to that of homopolymer electrolytes.[24] In the simplest case, ion transport in these electrolytes is governed by three transport coefficients, and a thermodynamic factor, T_f: the three transport coefficients are ionic conductivity κ, the salt diffusion coefficient D, and the cation transference number with respect to the solvent velocity t_{+}^{0}.[25] These parameters have been determined for two SEO block copolymers.[26,27] SEO transport coefficients can also be predicted from the

transport coefficients of PEO using the effective-medium theory of Sax and Ottino.[7,28] Both sets of transport parameters can be used to predict limiting current using Newman's concentrated solution theory.[23,25,29,30] In this paper, we compare measured limiting current density in the twelve nanostructured electrolytes with predictions based on both approaches.

EXPERIMENTAL SECTION

Polymer synthesis

In this study, we used polystyrene-*block*-poly(ethylene oxide) copolymers (PS-PEO, or SEO), which were synthesized by anionic polymerization, as described in previous work.[31–34] Characteristics of the twelve electrolytes used are reported in Table 1: copolymer name, molecular weight of the PS block, molecular weight of the PEO block, polydispersity index in N-Methyl-2-pyrrolidone (NMP) with respect to a polystyrene standard, PDI, and salt concentrations and corresponding volume fraction PEO and LiTFSI, $\varphi_{EO+LiTFSI}$, as calculated based on partial molar volumes measured in Ref 35 as described in Ref 36. The salt concentration r is defined as the molar ratio between LiTFSI and EO monomer units in the block copolymer. All four polymers are above the threshold at which molecular weight is expected to significantly affect macroscopic ion transport properties.[33]

Table 1: Properties of SEO electrolytes used in this study.

Name	**M_{PS} [kg mol^{-1}]**	**M_{PEO} [kg mol^{-1}]**	**PDI**	r	**$\varphi_{EO+LiTFSI}$**
SEO(110-183)	110	183	1.10	0	0.62
				0.04	0.65
				0.085	0.67

				0.12	0.69
SEO(115-172)	115	172	1.10	0	0.59
				0.04	0.62
				0.085	0.65
				0.12	0.67
SEO(200-222)	200	222	1.08	0	0.52
				0.04	0.55
				0.085	0.58
				0.12	0.60
SEO(235-222)	235	222	1.05	0	0.48
				0.04	0.51
				0.085	0.54
				0.12	0.56

All electrolyte preparation and electrochemical cell assembly steps were performed in argon filled gloveboxes with less than 1 ppm of water and less than 1 ppm of oxygen to avoid contamination.

Electrolyte casting

Methods for electrolyte preparation and electrochemical cell fabrication closely mimic those previously reported.[34,37–40] The salt used in this study was lithium bis(trifluoromethanesulfonyl) imide (LiTFSI). The solvent was N-Methyl-2-pyrrolidone (NMP). This casting method results in freestanding electrolyte membranes 35-200 μm thick.

Ionic conductivity

Ionic conductivity measurements were performed using both aluminum|SEO|aluminum symmetric cells and lithium|SEO|lithium symmetric cells. Cells were assembled using one circular punch of an SEO electrolyte membrane with a diameter of 3/8 inches and two circular punches of electrode material with diameters of 5/16 inches. The two electrodes were either aluminum blocking electrodes or lithium metal non-blocking electrodes which were backed with nickel foil. The lithium metal was obtained from FMC. All reported electrochemical data is for cells at 90 °C. Complex electrochemical ac impedance spectra were acquired using a BioLogic VMP3 potentiostat for a frequency range from 1 MHz to 1 Hz at an amplitude of 40 mV. The data were analyzed in the form of Nyquist plots and the electrical equivalent circuits in Fig. 1 were used to fit the data and obtain the bulk impedance used to calculate the ionic conductivity, as well as the interfacial impedance. R1 and L1 represent the response of the external cables, R2 and Q2 represent the electrolyte, and R3 and Q3 represent the polymer/lithium interface.

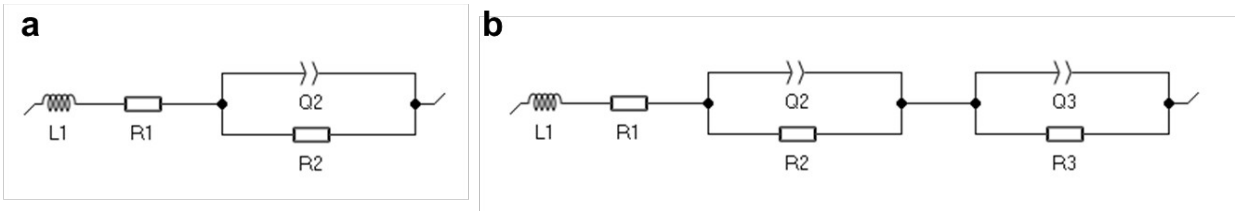

Figure 1. Electrical equivalent circuits used to fit Nyquist plots for cells with (a) aluminum blocking electrodes and (b) lithium non-blocking electrodes. R represents a resistor, L an inductor, and Q a constant phase element. L1 was restricted to be positive and R1 was set to 0.1 Ohms before fitting.

Restricted diffusion and steady-state current fraction

Steady-state current fraction and restricted diffusion measurements were performed using Li|SEO|Li symmetric cells (same assembly method as for ionic conductivity cells with lithium metal electrodes) and a BioLogic VMP3 potentiostat. Before measurements, cells were annealed for 1 h at 120 °C followed by 3 h at 110 °C. All measurements were performed at 90 °C. To

ensure stable interfacial layers at the lithium-polymer interfaces, 6 charge/discharge conditioning cycles at a low current density of 0.02 mA cm^{-2} were performed prior to the measurements. Each conditioning cycle consisted of a 4 h charge followed by a 45 min rest and a 4 h discharge followed by a 45 min rest. Ac electrochemical impedance spectroscopy was performed before polarization. The steady-state current fraction experiment consisted of applying a potential of ΔV = 20 mV and measuring the current at time intervals of 100 ms for 2 h, a time long enough to reach steady-state current. Ac impedance spectra were measured every 15 min. In the absence of a concentration gradient (i.e. prior to polarization), the calculated initial current, i_{Ω}, is defined by Ohm's law as given in Eq. 1, where ΔV is the difference between the potential response and the open-circuit voltage of the cell, and $R_{i,0}$ and $R_{b,0}$ are the initial resistances measured by ac impedance spectroscopy for the interface and the bulk respectively .[11]

$$i_{\Omega} = \frac{\Delta V}{R_{i,0} + R_{b,0}} \quad (1)$$

The current fraction, ρ_{+}, was calculated according to Eq. 2 as established by Evans, Bruce, and Vincent. $R_{i,SS}$ is the resistance of the interface at steady-state measured by ac impedance spectroscopy, and i_{SS} is the steady-state current.[8,9,11,41]

$$\rho_{+} = \frac{i_{SS}(\Delta V - i_{\Omega} R_{i,0})}{i_{\Omega}(\Delta V - i_{SS} R_{i,SS})} \quad (2)$$

Restricted-diffusion measurements of SEO electrolytes were performed immediately after the experiment to measure the current fraction. After a steady-state voltage response was reached, the cells were allowed to relax for up to 10 h under open-circuit voltage (OCV) conditions while the OCV, *U*, was recorded at time intervals of 500 ms. The data are fit to the functional form:

$$U(t) = k_0 + a e^{-bt} \quad (3)$$

where *a* and *b* are the fit parameters and k_0 is an empirically determined offset voltage. We posit that the offset voltage, k_0, arises from small temperature gradients in the symmetric cells due to the heating stage geometry.[42] The offset voltage is much smaller than *U* over most of the experimental window. The salt diffusion coefficient, D, is calculated using:

$$D = \frac{L^2 b}{\pi^2} \quad (4)$$

where *b* is from the fit of Eq. 3 and *L* is the thickness of the electrolyte as measured with a micrometer before cell fabrication.[42–44] The lower limits of the fits are such that $Dt/L^2 > 0.05$.

Limiting current density

The procedure to measure limiting current density was inspired by that reported by Hudson.[22] To ensure stable interfacial layers at the lithium-polymer interfaces, 6 charge/discharge conditioning cycles at a low current density of 0.02 mA cm^{-2} were performed prior to the measurements. Each conditioning cycle consisted of a 4 h charge followed by a 45 min rest and a 4 h discharge followed by a 45 min rest. To determine the limiting current density, lithium symmetric cells were polarized at a range of current densities. All experiments were conducted at 90 °C. Cells were first polarized in the positive and negative directions at 0.02, 0.05, and 0.08 mA cm^{-2} to establish the linear regime for the current-voltage relationship. During this step, each cell was polarized in one direction for 15 minutes, followed by a 15 min open circuit step to allow for relaxation, followed by 15 minutes of polarization in the opposite direction and then the same open circuit step. Following this initial characterization, a constant current density was applied to the cell and the resulting potential was measured. One of three

outcomes was observed: (1) the potential reached a steady-state value, (2) the potential diverged to infinity such that it would not reach a steady-state potential, or (3) the result was inconclusive. Once one of the outcomes was determined, the applied current was stopped and the cell was allowed to relax back to its equilibrium concentration gradient for at least 10 minutes. Polarization time was minimized to reduce the influence of dendritic growth on our measurements. In order to reduce polarization time at high current densities, we first sought an unsustainable current density i.e. one for which the voltage diverged. Following that, the highest sustainable current density was sought. Previous measurements informed the initial guesses of current densities to apply in each case. Once upper and lower bounds were established, intermediate current densities were tested in order to narrow the range of the bounds to less than 0.05 mA cm^{-2} or the cell failed by dendritic short-circuit. The direction of the applied current was alternated between each step to prolong cell lifetime. The true limiting current of the cell was taken to be within the range of the largest current applied which resulted in a steady-state potential and the smallest current applied which caused a divergence in potential. The points plotted as the limiting current are the average midpoints of this current range for at least three cells. The error bars represent the average upper bound and lower bound current densities. Electrochemical impedance spectroscopy was performed between each current step to ensure that bulk and interfacial impedances remained constant. After experimentation, these pouch cells were opened inside a glovebox, and a portion of the symmetric cell was cut out, re-pouched, and imaged by X-ray microtomography to determine electrolyte thickness, L. L corresponds to the average distance between approximately parallel electrodes, where the average was determined using at least 10 points within the cell using ImageJ on tomographic cross-sections of each cell.

X-ray microtomography

The cells were imaged using hard X-ray microtomography at the Advanced Light Source at Lawrence Berkeley National Laboratory – details can be found in the Supporting Information. The software Xi-Cam[45] and a Python script were used to create a 3D reconstruction of the cell. Cells were imaged in their original pouches at 4x magnification, corresponding to a pixel size of approximately 1.625 μm. Cross-sectional slices were stacked and rendered by the software ImageJ to take measurements of electrolyte thickness.

Electron microscopy

Scanning Electron Microscopy (SEM) was used to examine the microphase-separated morphology of the polymer electrolytes. Samples were prepared for microscopy in a method analogous to electrolyte membrane casting. The SEO block-copolymer was dissolved in NMP and mixed with LiTFSI such that the salt concentration r were equal to 0.04, 0.085 or 0.12. Then each solution was drop-cast on a silicon wafer. The solvent was evaporated at 60 °C on a casting plate, and then the samples were dried at 90 °C under active vacuum for 3 days prior to the experiment. Samples were transferred to the SEM facility using an air-tight desiccator. To prevent charging artefacts, a Gatan Sputter Coater was used to coat all samples with an approximately 2 nm thick carbon layer. The morphology of the samples was investigated using a FEI Helios G4 UX scanning electron microscope operated at 2 kV. Secondary electron images were acquired using the through-lens detector.

RESULTS AND DISCUSSION

I. Limiting Current Density Experiments

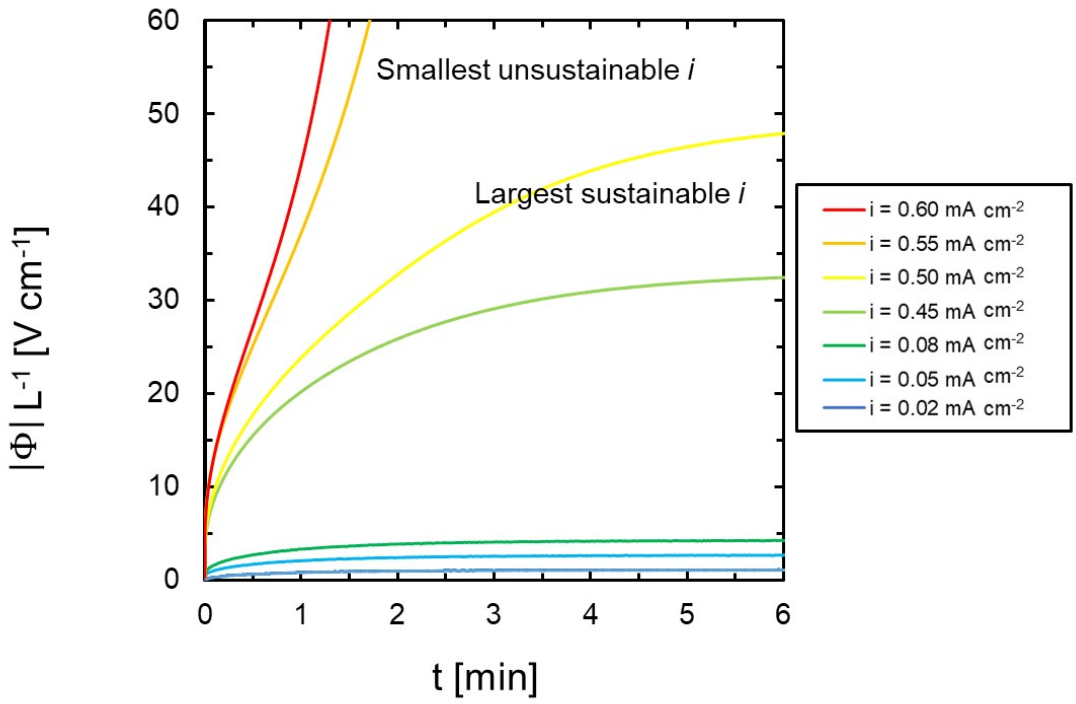

Figure 2. Absolute value of the length-normalized potential across the electrolyte as a function of time for different applied current densities. The measured potential was corrected to account for the potential drop due to interfacial impedances at the electrode/electrolyte interfaces and normalized by electrolyte thickness. These steps were conducted on one cell with the electrolyte SEO(235-222), $\varphi_{EO}=0.48$, $r=0.04$, and $L=43\,\mu m$ at 90 °C.

Typical results of the experiments used to determine the limiting current density are shown in Fig. 2. These steps were conducted on one cell with the electrolyte SEO(235-222), $\varphi_{EO}=0.48$, $r=0.04$, and $L=43\,\mu m$. Cells were polarized at a fixed current density and the potential response was measured as a function of time. The potential drop across the electrolyte, Φ, was calculated from the absolute potential response by subtracting the potential drop due to interfacial impedance as measured by ac impedance spectroscopy.[23,30] At low current densities (below 0.50 mA cm^{-2}), the potential reaches a plateau in about four minutes. The largest sustainable current density for this cell is 0.50 mA cm^{-2}. Increasing the current density to 0.55 mA cm^{-2} results in a qualitatively different behavior and the voltage versus time data exhibit an

inflection beyond which the voltage increases rapidly as a function of time. We take this to be the signature that the limiting current density has been exceeded, *i.e.*, the Li^+ redox reaction at the cathode is compromised because the salt concentration is close to zero. The smallest unsustainable current density for this cell is 0.55 mA cm^{-2}. We conclude that for the particular cell in Fig. 2, the limiting current density is 0.525 ± 0.025 mA cm^{-2}. Such experiments were repeated for all of the electrolytes in Table 1.

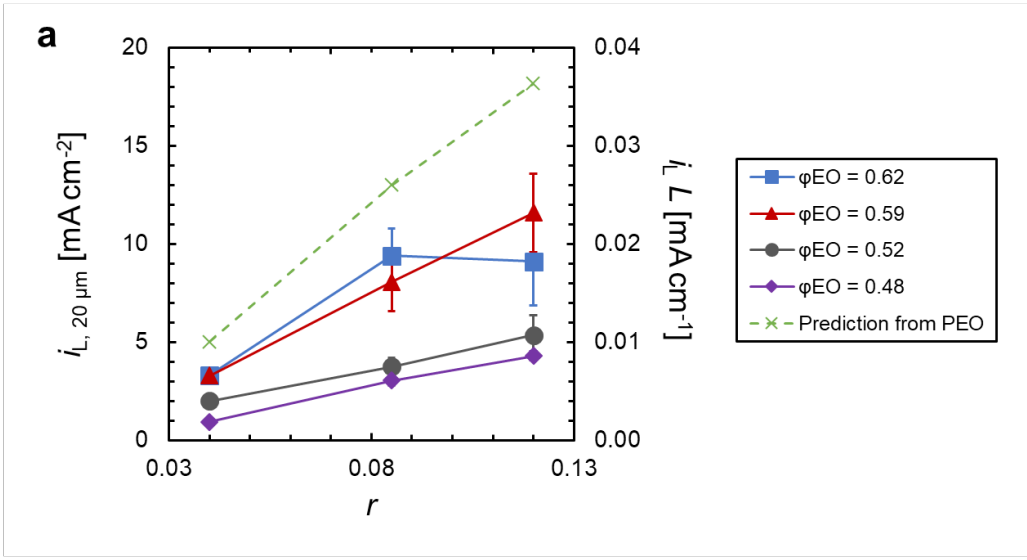

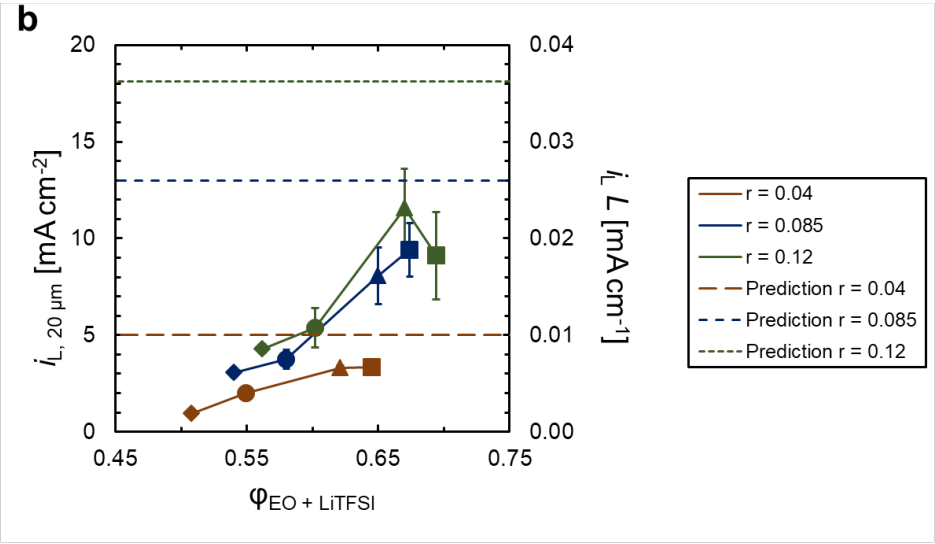

Figure 3. Limiting current density normalized to a 20 μm electrolyte thickness, $i_{L,20\,\mu m}$ (left *y*-axis), and limiting current density multiplied by thickness, $i_L L$ (right *y*-axis), for a series of SEO electrolytes at 90 °C. The dashed lines represent the prediction for limiting current density based on the transport properties of PEO taken from Ref. 23 and a lamellar morphology factor according to effective-medium theory. (a) Limiting current density plotted as a function of salt concentration in the conducting phase. (b) Limiting current densities plotted as a function of conducting volume fraction $\varphi_{EO+LiTFSI}$.

Fig. 3a plots the experimental results of limiting current density measurements on the series of SEO electrolytes given in Table 1 as a function of salt concentration, r. The left vertical axis represents the limiting current density normalized to an electrolyte thickness of 20 μm, $i_{L,20\,\mu m}$, while the right vertical axis represents limiting current density multiplied by thickness, $i_L L$. We chose 20 μm as it is a typical thickness for a battery separator. The solid lines represent four different SEO copolymers, characterized by the volume fraction of PEO in the block copolymer without salt, φ_{EO}, at three salt concentrations. Generally, i_L increases linearly with salt concentration. This is consistent with the expression for limiting current density in homogenous dilute electrolytes with concentration-independent transport properties:[46]

$$i_L = \frac{2cDF}{L\,¿¿}$$
¿

where c is the average concentration of salt in the electrolyte, D is the salt diffusion coefficient, F is the Faraday constant, L is the electrolyte thickness, and $t_{+¿¿}$ is the cation transference number. The relationship between c and r for a homopolymer electrolyte and a microphase separated electrolyte, is the same and is defined as the concentration of salt in the ion-conducting phase:[27]

$$c(r) = \frac{\rho(r)r}{M_{EO} + r\,M_{LiTFSI}} \quad (6)$$

where, $\rho(r)$ is the density of the PEO conducting phase[27], r is the molar ratio of lithium ions to ethylene oxide (EO) moieties, M_{EO} and M_{LiTFSI} are the molar masses of the EO unit (44.05 g mol^{-1}) and LiTFSI (287.08 g mol^{-1}), respectively.

Limiting current density measurements in PEO/LiTFSI homopolymer electrolytes reported by Gribble *et al.*[23] can be used to estimate the limiting current density in SEO/LiTFSI electrolytes. Concentration polarization in symmetric cells can be rigorously predicted using concentrated solution theory using Eq. 7,[30,47]

$$\int_{r(x=0)}^{r(x)} \frac{D(r)c(r)}{r\,t_{-¿^0(r)}}\,dr = \frac{-iL}{F}\left(\frac{x}{L}\right). ¿ \quad (7)$$

where $r(x)$ is the unitless molar ratio of salt in the electrolyte as a function of interelectrode distance, x, $D(r)$ is the salt diffusion coefficient as a function of r, $c(r)$ is defined in Eq. 6, i is the current density, L is the electrolyte thickness, and $t_{-¿^0¿}$ is the rigorously defined anion transference number with respect to solvent velocity.[25] Effective-medium theory can be used to relate transport parameters in homopolymer and block copolymer electrolytes as described by Hallinan *et al.*[7,28] This effective-medium theory framework was developed by Sax and Ottino and is valid when the transport path is much larger than the grain size and when the resistance to transport between grains is negligible.[28] Hallinan *et al.* proposed the following relationship between a diffusion coefficient in a composite electrolyte with one conducting domain, in this case D_{SEO}, compared to the diffusion coefficient in the conducting phase, in this case D_{PEO}, where f represents the form factor and τ represents the tortuosity factor:[7]

$$D_{SEO} = \frac{f}{\tau} D_{PEO} \quad (8)$$

In the case of a collection of randomly oriented lamellar grains, the simplest model gives $f=\frac{2}{3}$ and $\tau=1$.[28]

When we incorporate the effect of morphology on the diffusion coefficient according to effective-medium theory in Eq. 8, we see that

$$\frac{f}{\tau}\int_{r(x=0)}^{r(x)}\frac{D_{PEO}(r)c(r)}{r t_{-}^{0}(r)}dr=\frac{-iL}{F}\left(\frac{x}{L}\right). \quad (9)$$

We assume that the transference number is a function of the conducting phase composition only and is independent of block copolymer morphology. Thus, we may approximate the limiting current density of SEO as follows:

$$i_{L,SEO}=\frac{f}{\tau}i_{L,PEO} \quad (10)$$

The dashed green line in Fig. 3a represents Eq. 10 with $f=\frac{2}{3}$, $\tau=1$, and $i_{L,PEO}$ taken from Ref. 23. In that reference, it was shown that experimentally measured $i_{L,PEO}$ were in excellent agreement with theoretical predictions based on independently measured transport properties. This work was limited to the salt concentration range $0<r<0.085$. The green × symbols in Fig. 3a are based on the theoretical calculations in Ref. 23; the value at $r=0.12$ was obtained by linear extrapolation of results obtained at $r=0.065$ and $r=0.085$. It is clear that the effective-medium theory estimate of SEO limiting current density overpredicts the true, measured value.

Many transport properties of block copolymer electrolytes depend on the volume fraction of the conducting phase, $\varphi_{EO+LiTFSI}$. However, the limiting current density is predicted to be independent of this parameter (see Eq. 10). In Fig. 3b, we plot i_L versus $\varphi_{EO+LiTFSI}$. The left vertical axis represents the limiting current density normalized to an electrolyte thickness of 20

μm, $i_{L,20\,\mu m}$, while the right vertical axis represents limiting current density multiplied by thickness, $i_L L$. The dashed lines reflect the limiting current density predictions from Eq. 10. The effective-medium theory prediction is a function of the salt concentration in the conducting phase, and not of the conducting volume fraction. Experimentally, we see a significant dependence on conducting volume fraction, and the measured limiting currents begin to approach the predictions as conducting volume fraction increases.

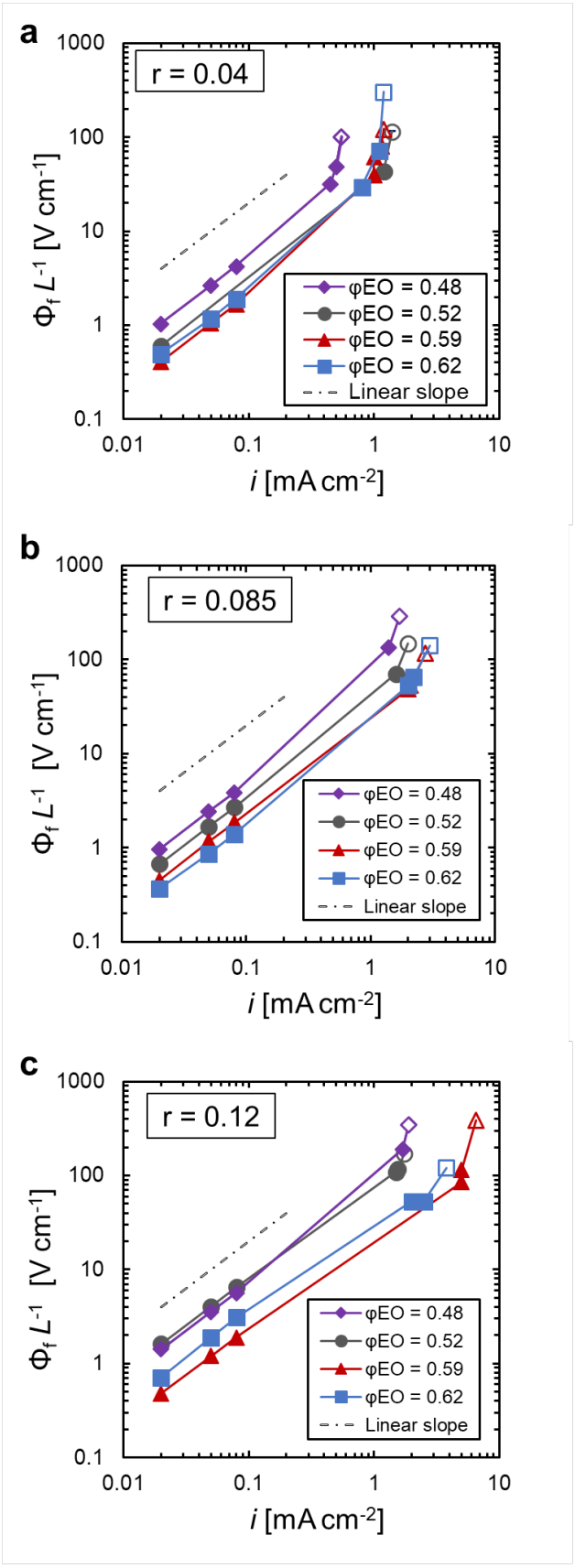
a
r = 0.04
b
r = 0.085
c
r = 0.12
φEO = 0.48
φEO = 0.52
φEO = 0.59
φEO = 0.62
Linear slope
Φf L-1 [V cm-1]
i [mA cm-2]
1000
100
10
1
0.1
0.01
0.1
1
10

Figure 4. Relationship between length-averaged steady-state potential across the electrolyte, $\Phi_f L^{-1}$, and current density, i, for each electrolyte in Table 1 at 90 °C for (a) $r=0.04$, (b) $r=0.085$, and (c) $r=0.12$. The filled symbols represent current densities at which a steady-state voltage was reached. The unfilled plotted point at the highest potential represents the potential at the end of the step where the lowest unsustainable current density was imposed. A linear slope on the log-log plot is shown as the dashed double line for reference; the data are generally parallel to this line, indicating a linear relationship between $\Phi_f L^{-1}$ and i.

Fig. 4 shows cell data obtained at current densities,i, below i_L as well as one point representing the voltage response to a current density above i_L. For each applied i, the measured steady-state potential response was processed to remove the potential drop across the interfaces and normalized by interelectrode distance L. The normalized value $\Phi_f L^{-1}$ is plotted. For each concentration, we show data obtained from one particular cell for each electrolyte. To a good approximation, $\Phi_f L^{-1}$ is a linear function of i below the limiting current. In most cases, a linear relationship is observed over a wide range of current densities $0<\frac{i}{i_L}<0.9$. Similar behavior has been seen in PEO/LiTFSI electrolytes.[23]

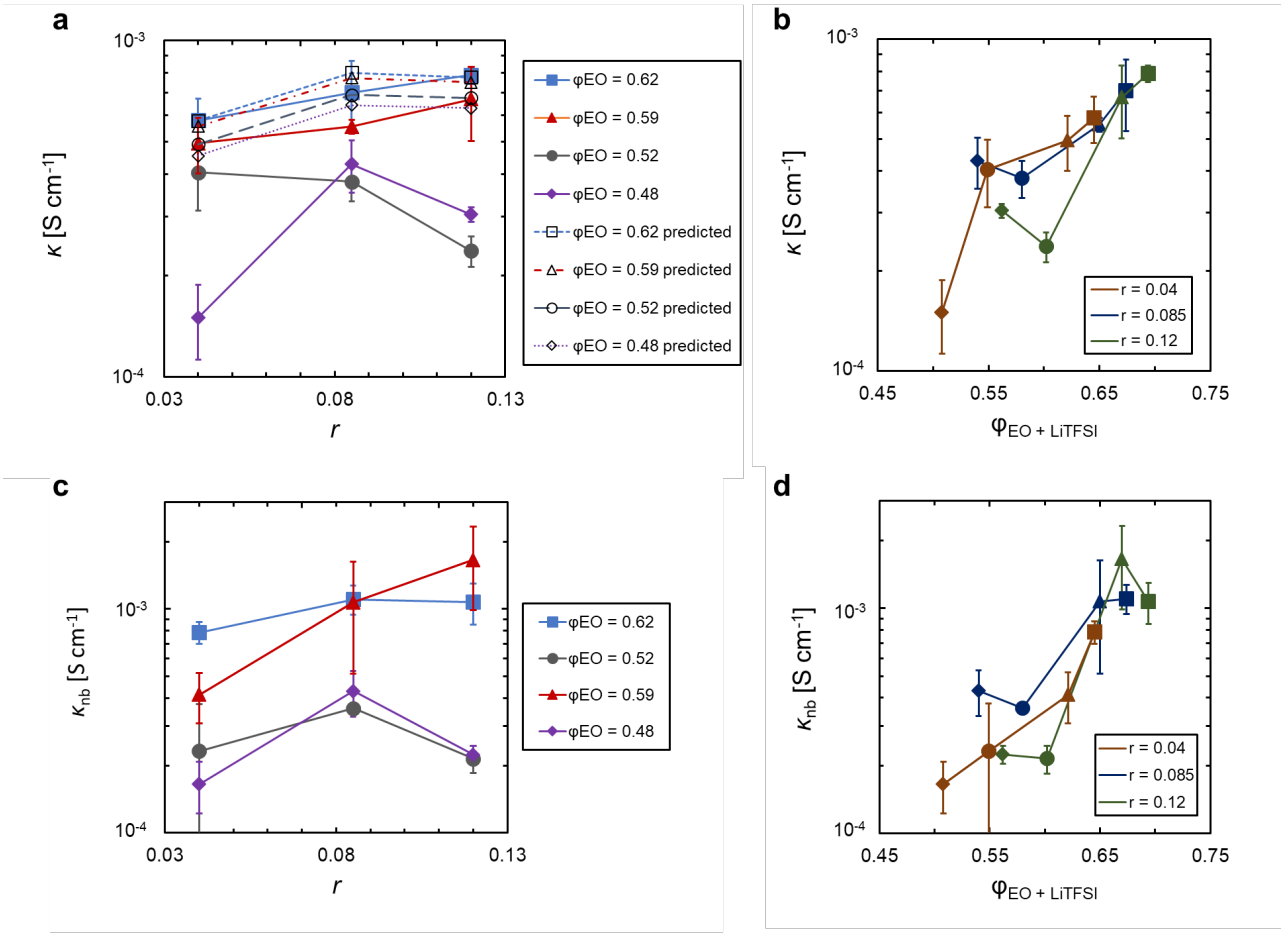

Figure 5. Ionic conductivity measured by ac impedance spectroscopy using blocking aluminum electrodes, κ, and non-blocking lithium electrodes, κ_{nb}, at 90 °C. (a) κ as a function of salt concentration r, (b) κ as a function of conducting volume fraction $\varphi_{EO+LiTFSI}$, (c) κ_{nb} as a function of salt concentration r, (d) κ_{nb} as a function of conducting volume fraction $\varphi_{EO+LiTFSI}$. Dashed lines in (a) represent predictions based on Eq. 11 and the ionic conductivity of homopolymer PEO electrolytes.[23] Note the values of κ_{nb} are higher than those of κ, and the y-axis scale differs.

The current versus voltage characteristics of an electrolyte can, in principle, be predicted by concentrated solution theory if all of the transport parameters and the thermodynamic factor are measured. We thus measured these properties independently in our block copolymer electrolytes. Ionic conductivity was measured by ac impedance spectroscopy using blocking aluminum electrodes, κ, and non-blocking lithium electrodes, κ_{nb}. Fig. 5a plots κ as a function of

salt concentration r for all twelve electrolytes. Effective-medium theory predicts that κ_{SEO} is given by[7]

$$\kappa_{SEO} = \frac{f}{\tau} \varphi_{EO+LiTFSI} \kappa_{PEO} \quad (11)$$

where κ_{SEO} is the ionic conductivity of the SEO electrolyte and κ_{PEO} represents the ionic conductivity of a PEO electrolyte of the same salt concentration. Dashed lines in Fig. 5a represent predictions based on Eq. 11, where the ionic conductivity of the homopolymer PEO electrolyte is taken from the polynomial fit through the data in Fig. 3a of Gribble *et al.*[23] See Supporting Information for further details. Agreement between κ and these predictions improves as $\varphi_{EO+LiTFSI}$ increases. The measured κ of the SEO samples with φ_{EO} of 0.62 and 0.59 are in quantitative agreement with predictions based on Eq. 11. Significant deviations are seen in SEO φ_{EO} = 0.52, particularly at r = 0.12. The largest deviations are seen in the sample with φ_{EO} of 0.48 at r = 0.04. Fig. 5b plots κ as a function of conducting volume fraction, $\varphi_{EO+LiTFSI}$. The data from all the samples collapse, except for $\varphi_{EO+LiTFSI}$ = 0.60 and r = 0.12.

Fig. 5c plots κ_{nb} as a function of salt concentration, r, and Fig. 5d plots κ_{nb} as a function of conducting volume fraction; these data were obtained by ac impedance spectroscopy using non-blocking lithium electrodes. For these electrolytes, κ_{nb} is generally higher than κ, with $\frac{\kappa_{nb}}{\kappa}$ equal to 1.2 on average and ranging between 0.74 and 2.5. While we do not know the reason for the difference between κ_{nb} and κ, discrepancies between them are common.[11] As seen in Figs. 5b and 5d, ionic conductivity increases with conducting phase volume fraction, as expected. The collapse of the data in Fig. 5d is noteworthy.

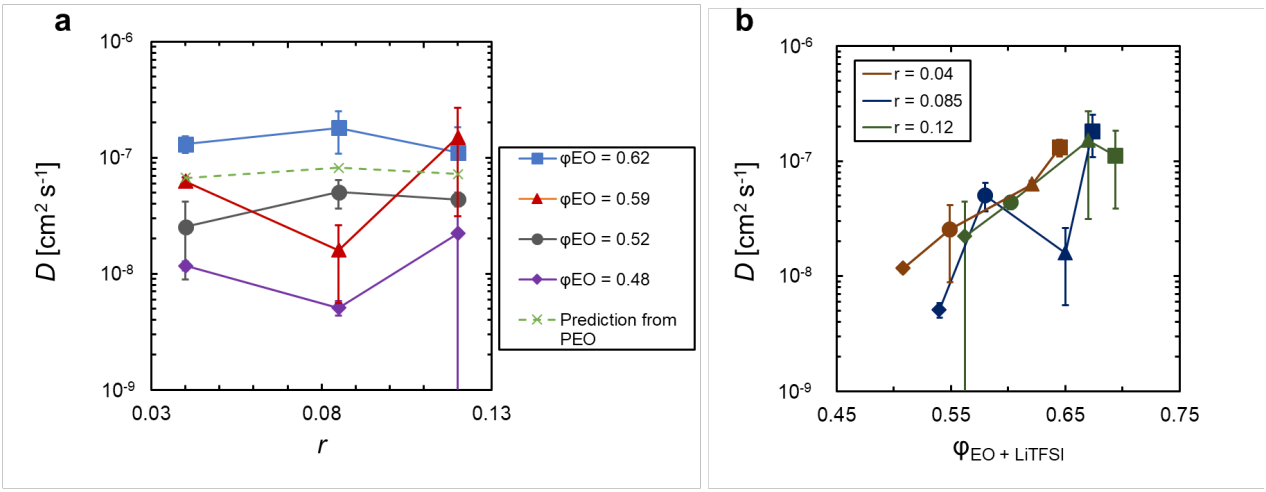

Figure 6. Restricted diffusion coefficients of SEO electrolytes, D, (a) as a function of salt concentration, r, and (b) as a function of conducting volume fraction, $\varphi_{EO+LiTFSI}$, at 90 °C. The dashed line in (a) represents predictions based on Eq. 8 and the restricted diffusion coefficient of homopolymer PEO electrolytes.[23]

The mutual diffusion coefficients of salt in our electrolytes, D, were measured by the restricted diffusion technique.[42–44] Fig. 6a plots D as a function of salt concentration r. The dashed lines in Fig. 6a connect predictions based on effective-medium theory, *i.e.* Eq. 8 and the salt diffusion coefficient of homopolymer PEO electrolytes;[7] D is predicted to be independent of $\varphi_{EO+LiTFSI}$. The diffusion coefficient of LiTFSI in homopolymer PEO electrolyte is taken from the polynomial fit through the data in Fig. 3b of Gribble *et al.*[23] The figure is reproduced in the Supporting Information of this manuscript for reference. The measured diffusion coefficients are more or less independent of r as predicted by theory, but they decrease monotonically with decreasingφ_{EO}. At φ_{EO}= 0.62, the measured values are slightly higher than predictions. At φ_{EO}= 0.59, only the electrolyte at r = 0.085 has a diffusion coefficient significantly below the prediction. At φ_{EO} = 0.48, all of the measured values of D are below effective medium theory predictions.

Fig. 6b plots D as a function of conducting volume fraction $\varphi_{EO+LiTFSI}$ and shows that D increases with $\varphi_{EO+LiTFSI}$. When the data are plotted using these axes, we observe a collapse from most of the samples (all of the samples, except r = 0.085 and $\varphi_{EO+LiTFSI}$ = 0.65). Fig. 6b reveals a trend which is inconsistent with effective medium theory. Such inconsistencies may arise due to effects not included in effective-medium theory, such as resistance to ion transport at grain boundaries.[48]

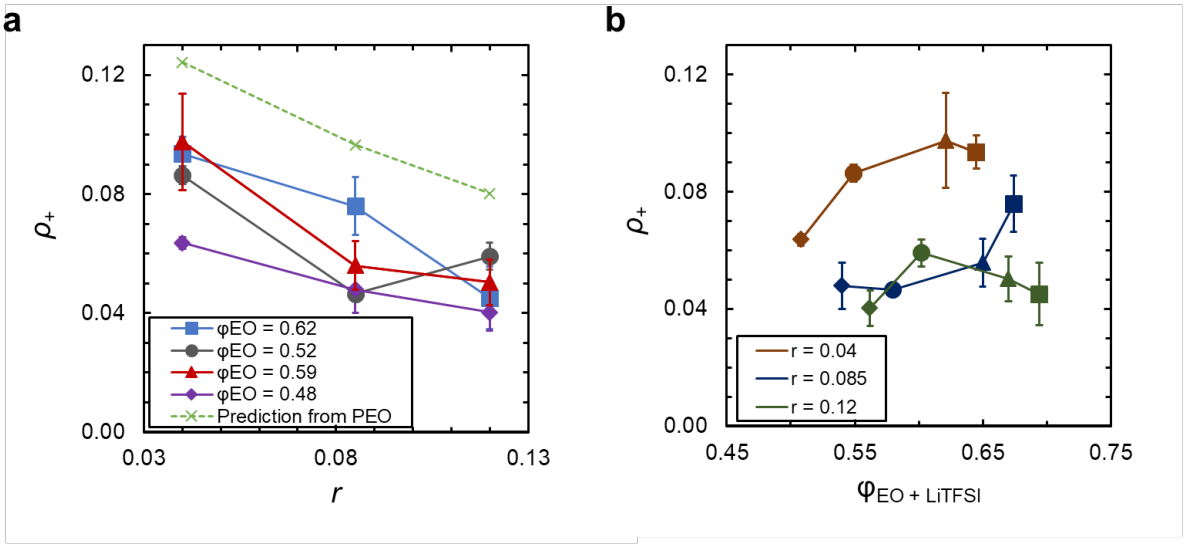

Figure 7. Steady-state current fraction of SEO electrolytes, $\rho_{+¿¿}$, (a) as a function of salt concentration r, and (b) as a function of conducting volume fraction $\varphi_{EO+LiTFSI}$ at 90 °C. The legend differentiates polymers based on the volume fraction of PEO in the block copolymer without salt, φ_{EO}, referenced in Table 1 or by salt concentration. The dashed line in (a) represents predictions based on Eq. 12 and the current fraction of homopolymer PEO electrolytes.[23]

The current fraction $\rho_{+¿¿}$ was measured for each electrolyte using the steady-state polarization technique pioneered by Evans, Bruce, and Vincent.[8,9,11] In the literature, $\rho_{+¿¿}$ has been referred to as the transference number. The transference number and $\rho_{+¿¿}$ are only equal to each other in dilute electrolytes that are thermodynamically ideal. None of the electrolytes of interest here satisfy these conditions.

Fig. 7a plots $\rho_{+,,}$ as a function of salt concentration r. The dashed line in Fig. 7a represents the predictions of effective-medium theory for current fraction:

$$\rho_{+,SEO} = \rho_{+,PEO} \quad (12)$$

and $\rho_{+,PEO}$ as a function of r is taken from Ref. 23. The current fraction in homopolymer PEO electrolytes is taken from the polynomial fit through the data in Fig. 3c of Gribble *et al.*[23] The figure is reproduced in the Supporting Information of this manuscript for reference. If effective-medium theory were a valid approximation, $\rho_{+,,}$ data from the four different block copolymers and the homopolymer would collapse on to a single curve. This is clearly not the case.

In all of the block copolymers, $\rho_{+,,}$ decreases with r, consistent with the prediction of effective medium theory. The magnitude of the decrease is also consistent with this prediction. However, the overall values in these high molecular weight SEO electrolytes are significantly lower than the predictions. The reason for this remains to be established. In Fig. 7b, we plot $\rho_{+,,}$ as a function of $\varphi_{EO+LiTFSI}$. At r = 0.04 and 0.085, $\rho_{+,,}$ increases with $\varphi_{EO+LiTFSI}$. At r = 0.12, $\rho_{+,,}$ is a weak function of $\varphi_{EO+LiTFSI}$ and ranges from 0.04 to 0.06 across the accessible window.

Although PEO and lower molecular weight SEO polymer electrolytes have been reported to have similar values of $\rho_{+,,}$, $\rho_{+,,}$ appears to be consistently lower for high molecular weight SEO polymer electrolytes.[27,49] We do note that $\rho_{+,SEO}$ decreases with increasing r, as is the case for $\rho_{+,PEO}$. Fig. 7b plots $\rho_{+,,}$ as a function of conducting volume fraction $\varphi_{EO+LiTFSI}$. Comparing Fig. 7a and 7b, we conclude that $\rho_{+,,}$ is primarily determined by r, not $\varphi_{EO+LiTFSI}$. This is in agreement with previous measurements.[49]

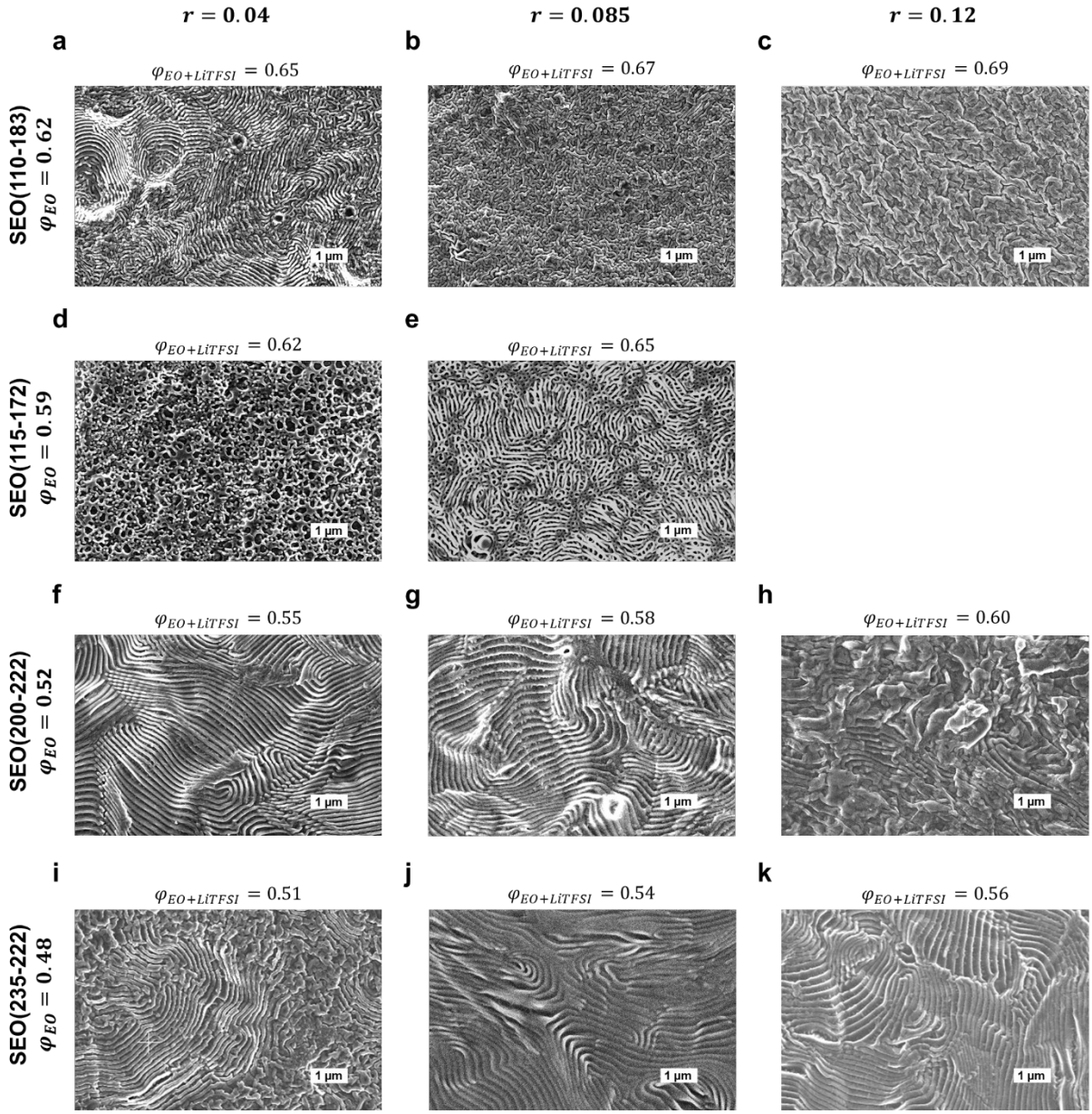

Figure 8. SEM micrographs of the surfaces of SEO electrolyte membranes. All scale bars represent 1 µm. (a-c) represent electrolytes from the polymer SEO(110-183) with φ_{EO}=0.62, (d,e) represent electrolytes from the polymer SEO(115-172) with φ_{EO}=0.59, (f-h) represent electrolytes from the polymer SEO(200-222) with φ_{EO}=0.52, and (i-k) represent electrolytes from the polymer SEO(235-222) with φ_{EO}=0.48. The leftmost column of images represents electrolytes with r=0.04, the center column represents electrolytes with r=0.085, and the rightmost column of images represents electrolytes with r=0.12.

Scanning electron microscopy (SEM) was used to provide information about the morphology of the electrolytes. As determined by SEM, the overall microstructures of the top

surfaces were heterogeneous, with lamellar regions in most samples. For comparison, Fig. 8 presents micrographs from select regions on the surface of each electrolyte membrane that provide a qualitative comparison between systems at a similar length scale. As shown, the lamellar thicknesses of these selected regions in the SEO(110-183) and SEO (115-172) are smaller than those of SEO(200-222) and SEO (235-222). This is expected because the total molar mass of the first two polymers is about 300 kg mol^{-1}, while that of the latter two polymers exceeds 400 kg mol^{-1}. The grain structure in these electrolytes is complex. Generally speaking, larger grains are seen in SEO(200-222) and SEO(235-222). We note that the greatest deviations from effective-medium theory are also seen in these two polymers. For example, the ionic conductivity of these polymers lie well below effective-medium theory prediction, while those of SEO(110-183) and SEO(115-172) with $\varphi_{EO}=0.59$ and $\varphi_{EO}=0.62$ are roughly consistent with predictions (see Fig. 5a).

We use concentrated solution theory[25] along with the methodology developed by Pesko *et al.*[30] to predict the limiting current densities of our 12 electrolytes.[23] As defined before, the limiting current is obtained when the salt concentration at the cathode approaches zero. It is possible to calculate steady-state salt concentration profiles, $r(x)$, across the cell by employing measured transport properties of the electrolyte. The salt concentration profile in a symmetric cell is governed by the following expression[50]:

$$\int_{r(x=0)}^{r(x)} \frac{\kappa}{\text{¿¿}}\,\text{¿}$$

where κ is the ionic conductivity, $\rho_{+\text{¿¿}}$ is the current fraction, $z_{+\text{¿}=1\text{¿}}$ is the charge number for LiTFSI, $\nu_{+\text{¿}=1\text{¿}}$ is the number of cations for LiTFSI, F is the Faraday constant, $\varphi_{EO+LiTFSI}$ is the

volume fraction of the conducting phase, m is the molality of salt in the conducting phase, and $\frac{dU}{dlnm}$ is the change in the open circuit potential with respect to m. It is important to note that the rigorously defined cation transference number with respect to the solvent velocity, $t_{+¿^0¿}$, is used in the derivation of equation 13, as shown in Ref 50. The numerical values of $t_{+¿^0¿}$ are very different from $\rho_{+¿¿}$ due to the fact that our electrolyte is neither dilute nor thermodynamically ideal. Integrating Eq. 13 requires knowledge of the composition-dependent properties on the left side: κ, $\rho_{+¿¿}$, and $\frac{dU}{dlnm}$. We ignore, for simplicity, the dependence of $\varphi_{EO+LiTFSI}$ on r. The parameters $\rho_{+¿¿}$ and $\frac{dU}{dlnm}$ are weak functions of block copolymer composition and chain length.[49] We used the fitted expression of $\rho_{+¿¿}$ measured for φ_{EO}= 0.48 in Frenck *et al.* [50] for all SEO electrolytes. These parameters are shown in Eq. 14 and also given in Table 2. We use values reported for SEO electrolytes in Villaluenga *et al.*[27] for $\frac{dU}{dlnm}$ shown in Eq. 15:

$$\rho_{+¿}=5.49r^2-1.29r+0.11¿ \quad (14)$$

$$\frac{dU}{dln\,m}=5.31(\ln m)^2-89.62(\ln m)-82.69 \quad (15)$$

The dependence of κ of SEO block copolymer electrolytes on salt concentration has been established in the literature. The data for SEO(235-222) with $\varphi_{EO}=0.48$ is reported in Frenck *et al.*[50], while that for SEO (240-260) with $\varphi_{EO}=0.51$ is reported in Villaluenga *et al.*[27] The conductivity of SEO(110-183), SEO(115-172) and SEO(200-222) was measured at three salt concentrations. We assumed that the polynomial dependence of κ on r was the same for similar

polymers. For SEO(200-222), a constant was added to the polynomial fit through the conductivity data reported for SEO(235-222) in Ref. [50]. For SEO(110-183) and SEO(115-172), a constant for each polymer was added to the polynomial fit through the conductivity data reported in Ref. 27. In both studies the constants were chosen to minimize the deviation between the fits and the conductivity data. All fitting parameters for κ are reported in Table 2. All of these results can be combined to obtain the functional form of the integrand in Eq. 13:

$$\frac{\kappa}{\dot{\iota}\dot{\iota}\dot{\iota}}$$

Table 2. Fitting parameters used for κ, $\frac{\kappa}{\dot{\iota}\dot{\iota}}$ and $\rho_{+\dot{\iota}\dot{\iota}}$ for each SEO electrolyte.

φ_{EO}	***Property***	***a***	***b***	***c***	***d***	***e***	***f***	***g***
0.62	κ				$7.92\ 10^{-2}$	$-4.79\ 10^{-2}$	$8.6\ 10^{-3}$	$1.2\ 10^{-4}$
	$\frac{\kappa}{\dot{\iota}\dot{\iota}}$	$-5.60\ 10^{-4}$	$4.94\ 10^{-4}$	$-1.74\ 10^{-5}$	$3.12\ 10^{-5}$	$-2.91\ 10^{-6}$	$1.25\ 10^{-7}$	$-1.02\ 10^{-9}$
0.59	κ				$7.92\ 10^{-2}$	$-4.79\ 10^{-2}$	$8.6\ 10^{-3}$	$2.5\ 10^{-4}$
	$\frac{\kappa}{\dot{\iota}\dot{\iota}}$	$-7.04\ 10^{-4}$	$6.16\ 10^{-4}$	$-2.15\ 10^{-4}$	$3.79\ 10^{-5}$	$-3.46\ 10^{-6}$	$1.43\ 10^{-7}$	$-9.43\ 10^{-10}$
0.52	κ			$-8.28\ 10^{-1}$	$6.88\ 10^{-1}$	$1.96\ 10^{-1}$	$2.11\ 10^{-2}$	$-3.61\ 10^{-4}$
	$\frac{\kappa}{\dot{\iota}\dot{\iota}}$	$-5.83\ 10^{-4}$	$5.33\ 10^{-4}$	$-1.96\ 10^{-4}$	$3.68\ 10^{-5}$	$-3.67\ 10^{-6}$	$1.78\ 10^{-7}$	$-2.57\ 10^{-9}$
0.48	κ			$-8.28\ 10^{-1}$	$6.88\ 10^{-1}$	$1.96\ 10^{-1}$	$2.11\ 10^{-2}$	$4.41\ 10^{-4}$
	$\frac{\kappa}{\dot{\iota}\dot{\iota}}$	$-3.99\ 10^{-4}$	$3.80\ 10^{-4}$	$-1.46\ 10^{-4}$	$2.88\ 10^{-5}$	$-3.03\ 10^{-6}$	$1.55\ 10^{-7}$	$-2.59\ 10^{-9}$
all	$\rho_{+\dot{\iota}\dot{\iota}}$					5.49	-1.29	0.11

Table footnote: All polynomials are given in function of r. Units for ionic conductivity are S cm^{-1}, and units for $\frac{\kappa}{\dot{\iota}\dot{\iota}}$ are mol $cm^{-1}s^{-1}$.

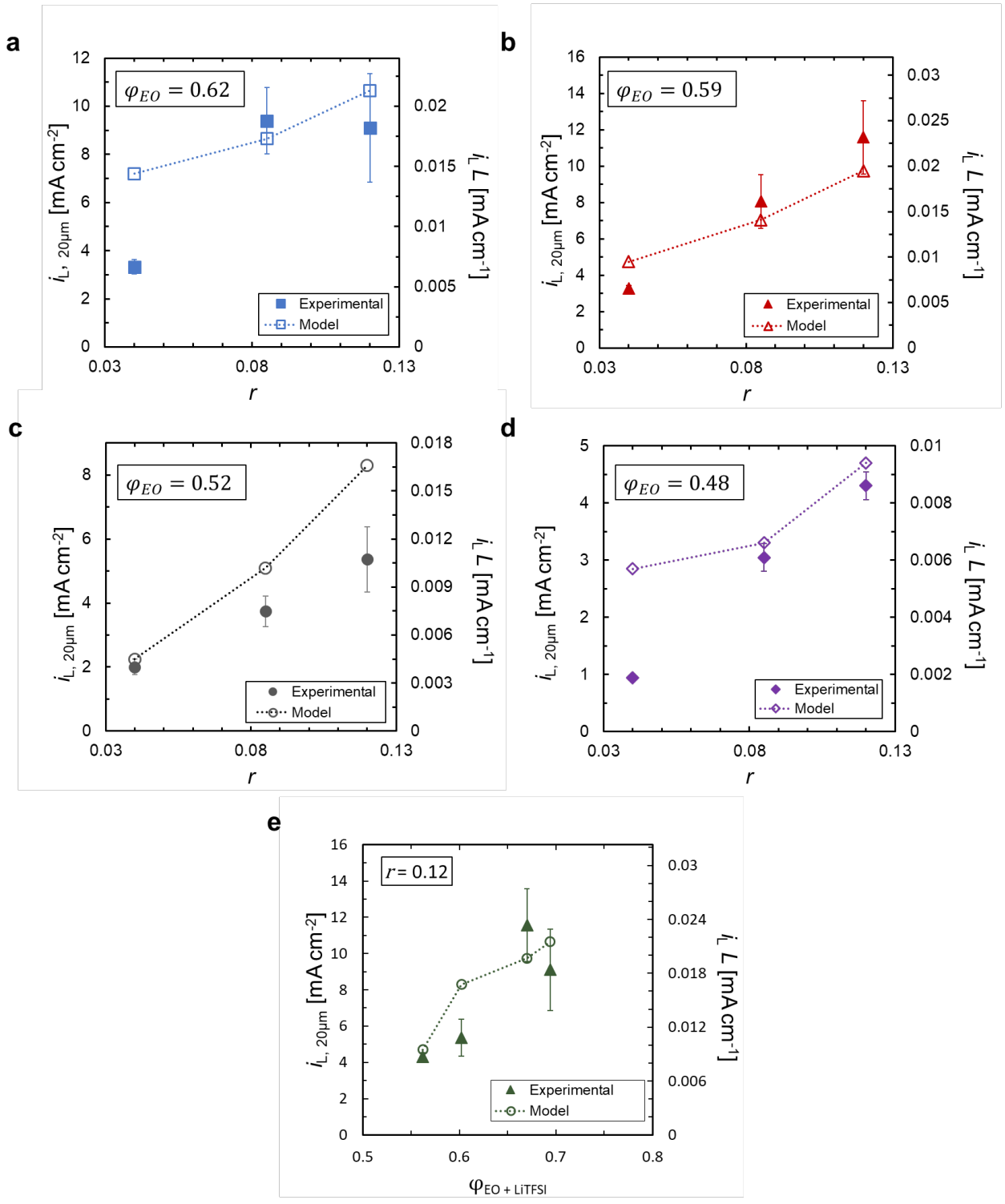

Figure 9. Comparison of SEO experimental limiting current to concentrated solution theory approximation based on characterization and concentrated solution theory approximation for

electrolytes containing (a) SEO(110-183) with $\varphi_{EO}=0.62$, (b) SEO(115-172) with $\varphi_{EO}=0.59$, (c) SEO(200-222) with $\varphi_{EO}=0.52$, and (d) SEO(235-222) with $\varphi_{EO}=0.48$ (d) Comparison of SEO experimental limiting current to concentrated solution theory for electrolytes containing $r=0.12$ in function of $\varphi_{EO+LiTFSI}$.

For an applied current density i, Eq. 13 was used to calculate the value of r at $x=L$ with the integrand given by Eq. 16 and parameters given in Table 2. The current density at which the calculated value of r at $x=L$ was zero was taken to be the limiting current density. In Fig. 9, we compare the experimentally measured limiting current densities with theoretical predictions. In many cases, we find quantitative agreement between theory and experiment. Significant departures are seen between theory and experiment in dilute electrolytes with $\varphi_{EO}=0.48$ and $\varphi_{EO}=0.62$. Departures are also seen at high concentration in electrolyte with φ_{EO} ¿ 0.52. In all cases where departure is observed, the experimentally measured limiting current lies below the theoretical prediction. More work is needed to explore the reason for this observation. What is clear however, is that the limiting current increases systematically with increasing φ_{EO}. At r = 0.12, the most concentrated electrolyte, the experimentally measured limiting current increases from 4.5 mA cm^{-2} to 10 mA cm^{-2} as shown in Fig. 9e. The observed factor of two increase of limiting current is perhaps surprising given the fact that φ_{EO} was changed modestly from 0.48 to 0.62. By and large, we conclude that concentrated solution theory, which was originally developed for characterizing ion transport in homogeneous electrolytes, applies remarkably well when used to predict the limiting current of nanostructured block copolymer electrolytes. In contrast, effective medium theory, which is widely used to interpret conductivity of block copolymer electrolytes, predicts that the limiting current is independent of $\varphi_{EO+LiTFSI}$.

CONCLUSION

Limiting current density is an important metric of battery electrolytes as it describes the highest rate of ion transport that can be accommodated by the electrolyte. Developing new electrolytes for lithium batteries is an active field of research, and comparisons are often based on conductivity and current fraction. We suggest that limiting current density is a simple metric for comparing the efficacy of different electrolytes. Herein, the limiting current density was measured for a series of twelve microphase separated PS-*b*-PEO block copolymer electrolytes. In this class of nanostructured electrolytes, the highest limiting current density measured was 11.6 mA cm^{-2} normalized to a 20 μm thick membrane. The limiting current increases with increasing φ_{EO}; φ_{EO} of the optimal block copolymer in our study was 0.59. The ionic conductivity, the mutual diffusion coefficient of lithium salt, and the current fraction were also measured and reported as functions of salt concentration and conducting phase volume fraction. The limiting current densities of these nanostructured electrolytes were compared to those of homopolymer PEO electrolytes using the effective medium theory put forth by Sax and Ottino. Our results are qualitatively inconsistent with effective medium theory, which predicts that limiting current is independent of φ_{EO}. Limiting current measurements were also compared to results from a model based on concentration solution theory using independently measured transport parameters. The estimate based on concentrated solution theory, which was originally developed for characterizing ion transport in homogenous electrolytes, was shown to apply remarkably well to these nanostructured electrolytes. Our approach provides a useful tool to predict limiting current

density in nanostructured electrolytes using readily measured transport parameters, which can in turn help design improved block copolymer electrolytes for battery applications.

ASSOCIATED CONTENT

Supporting Information. The following files are available free of charge.

Limiting current in block copolymer electrolytes SI (word)

AUTHOR INFORMATION

Corresponding Author

* E-mail: nbalsara@berkeley.edu. Phone: 1-510-642-8973

* Address: 201C Gilman Hall, Berkeley, CA 94720

ORCID

Jacqueline A. Maslyn: 0000-0002-6481-2070
Louise Frenck: 0000-0001-7116-2144
Vijay D. Veeraraghavan: 0000-0001-7327-7316
Alexander Müller: 0000-0002-8049-6610
Alec S. Ho: 0000-0003-1373-5332
Whitney S. Loo: 0000-0002-9773-3571
Dilworth Y. Parkinson: 0000-0002-1817-0716
Andrew M. Minor: 0000-0003-3606-8309
Nitash P. Balsara: 0000-0002-0106-5565

Author Contributions

J.A.M. and W.S.L. synthesized SEO block copolymer. J.A.M., L.F. and V.V. fabricated samples and performed the experiments. A.M. run scanning electron microscopy experiments. J.A.M., LF, D.Y.P. and A.S.H. aided in synchrotron experimental set-up and discussion of results. J.A.M., L.F. and N.P.B. prepared figures and composed the manuscript. N.P.B. directed the work.

Note

The authors declare no competing financial interest.

ACKNOWLEDGMENT

This work was supported by the Assistant Secretary for Energy Efficiency and Renewable Energy, Office of Vehicle Technologies of the U.S. Department of Energy under Contract DE-AC02-05CH11231 under the Advanced Battery Materials Research Program (BMR). JAM was supported by a National Science Foundation Graduate Research Fellowship DGE-2752814. LF acknowledges funding from the Energy & Biosciences Institute through the EBI-Shell program. X-ray experiments were performed at the Advanced Light Source which is supported by the Director, Office of Science, Office of Basic Energy Sciences, of the U.S. Department of Energy under Contract No. DE-AC02-05CH11231. ASH was supported by a National Science Foundation Graduate Research Fellowship DGE-2020294884. WSL was supported by a National Science Foundation Graduate Research Fellowship DGE-1106400. Work at the Molecular Foundry was supported by the Office of Science, Office of Basic Energy Sciences, of the U.S. Department of Energy under Contract No. DE-AC02-05CH11231.

ABBREVIATIONS

Abbreviations	
EO	Ethylene oxide
LiTFSI	lithium bis(trifluoromethanesulfonyl)imide
NMP	N-Methyl-2-pyrrolidone
OCV	Open circuit voltage
PDI	polydispersity index in NMP with respect to a polystyrene standard
PEO	Poly(ethylene oxide)

PS	Polystyrene
SEO	Poly(styrene)-*b*-poly(ethylene oxide)
SEM	Scanning electron microscopy
Symbol	
M_{LiTFSI}	Molecular weight of the lithium salt LiTFSI [kg mol^{-1}]
M_{PS}	Molecular weight of the polystyrene block [kg mol^{-1}]
M_{PEO}	Molecular weight of the poly(ethylene-oxide) block [kg mol^{-1}]
M_{EO}	Molecular weight of ethylene oxide [kg mol^{-1}]
T_{f}	Thermodynamic factor
i	Current density [mA cm^{-2}]
i_L	Limiting current density [mA cm^{-2}]
V	Voltage [V]
ϕ	Overpotential across electrolyte normalized by electrolyte thickness [V cm^{-1}]
r	Salt concentration in the PEO-rich phase, defined as the molar ratio, $\frac{[LiTFSI]}{[EO]}$
$t_{+¿¿}$	Dilute solution theory transference number of the cation
$t_{-¿^0¿}$	Concentrated solution theory transference number of the anion with respect to the solvent velocity; $t_{-¿^0}=1-t_{+¿^0¿}$
D	Salt diffusion coefficient [cm^2 s^{-1}]
c	Concentration of lithium salt in the conducting phase [mol cm^{-3}]
ρ	Density of the electrolyte [g cm^{-3}]
κ	Ionic conductivity measured in a cell with blocking electrodes [S cm^{-1}]
κ_{nb}	Ionic conductivity measured in a cell with non-blocking electrodes [S cm^{-1}]
$\rho_{+¿¿}$	Current fraction
$z_{+¿¿}$	Charge number of the cation
$v_{+¿¿}$	Number of cations in the dissociated salt

φ_c	Volume fraction of the conducting phase
φ_{EO}	Volume fraction of the PEO-rich phase
$\varphi_{EO+LiTFSI}$	Conducting volume fraction; volume fraction of the PEO-LiTFSI phase
$\frac{dU}{d\ln m}$	Change in open-circuit potential with respect to the logarithm of the molal concentration of salt in the electrolyte [V]
F	The Faraday constant [C mol^{-1}]
L	Electrolyte thickness [cm]
x	Position in the electrolyte [cm]
f	Form factor in effective-medium theory
τ	Tortuosity factor in effective-medium theory

REFERENCES

(1) Cheng, X.-B.; Zhang, R.; Zhao, C.-Z.; Zhang, Q. Toward Safe Lithium Metal Anode in Rechargeable Batteries: A Review. *Chem. Rev.* **2017**, *117*, 10403–10473. https://doi.org/10.1021/acs.chemrev.7b00115.

(2) Balsara, N. P.; Newman, J. Comparing the Energy Content of Batteries, Fuels, and Materials. *J. Chem. Educ.* **2013**, *90* (4), 446–452. https://doi.org/10.1021/ed3004066.

(3) Zhang, J.-G.; Wu, X.; Henderson, W. A. *Springer Series in Materials Science: Lithium Metal Anodes and Rechargeable Lithium Metal Batteries*; 2017.

(4) Aurbach, D. Review of Selected Electrode – Solution Interactions Which Determine the Performance of Li and Li Ion Batteries. **2000**, 206–218.

(5) Wood, K. N.; Noked, M.; Dasgupta, N. P. Lithium Metal Anodes: Toward an Improved Understanding of Coupled Morphological, Electrochemical, and Mechanical Behavior. *ACS Energy Letters*. American Chemical Society March 10, 2017, pp 664–672. https://doi.org/10.1021/acsenergylett.6b00650.

(6) Croce, F.; Appetecchi, G. B.; Persi, L.; Scrosati, B. Nanocomposite Polymer Electrolytes for Lithium Batteries. *Nature* **1998**, *394* (6692), 456–458. https://doi.org/10.1038/28818.

(7) Hallinan, D. T.; Villaluenga, I.; Balsara, N. P. Polymer and Composite Electrolytes. *MRS Bull.* **2018**, *43* (10), 775–781. https://doi.org/10.1557/mrs.2018.212.

(8) Evans, J.; Vincent, C. A.; Bruce, P. G. Electrochemical Measurement of Transference Numbers in Polymer Electrolytes. *Polymer (Guildf).* **1987**, *28* (13), 2324–2328. https://doi.org/10.1016/0032-3861(87)90394-6.

(9) Bruce, P. G.; Evans, J.; Vincent, C. A. Conductivity and Transference Number Measurements on Polymer Electrolytes. *Solid State Ionics* **1988**, *28–30* (PART 2), 918–922. https://doi.org/10.1016/0167-2738(88)90304-9.

(10) Gray, F. M.; Bruce, P. G. *Solid State Electrochemistry, Edited by P. G. Bruce (Cambridge University Press, 1995), Pp. 157–158.*

(11) Galluzzo, M. D.; Maslyn, J. A.; Shah, D. B.; Balsara, N. P. Ohm's Law for Ion Conduction in Lithium and beyond-Lithium Battery Electrolytes. *J. Chem. Phys.* **2019**, *151* (2), 020901. https://doi.org/10.1063/1.5109684.

(12) Hogge, E. A.; Kraichman, M. B. The Limiting Current on a Rotating Disc Electrode in Potassium Iodide-Potassium Triiodide Solutions. *J. Am. Chem. Soc.* **1954**, *76* (5), 1431–1433. https://doi.org/10.1021/ja01634a088.

(13) Tobias, C. W.; Eisenberg, M.; Wilke, C. R. Diffusion and Convection in Electrolysis—A Theoretical Review. *J. Electrochem. Soc.* **1952**, *99* (12), 359C-365C. https://doi.org/10.1149/1.2779636.

(14) Sand, H. J. S. On the Concentration at the Electrodes in a Solution, with Special Reference to the Liberation of Hydrogen by Electrolysis of a Mixture of Copper Sulphate and Sulphuric Acid. *Proc. Phys. Soc. London* **1899**, *17*, 496–534. https://doi.org/10.1088/1478-7814/17/1/332.

(15) Choo, Y.; Halat, D. M.; Villaluenga, I.; Timachova, K.; Balsara, N. P. Diffusion and Migration in Polymer Electrolytes. *Prog. Polym. Sci.* **2020**, *103*, 101220. https://doi.org/10.1016/j.progpolymsci.2020.101220.

(16) Selman, J. R.; Tobias, C. W. Mass-Transfer Measurements by the Limiting-Current Technique. *Adv. Chem. Eng.* **1978**, *10*, 211–318.

(17) Agar, J. N. Diffusion and Convection at Electrodes. *Discuss. Faraday Soc.* **1947**, *1*, 26–37.

(18) Shah, D. B.; Kim, H. K.; Nguyen, H. Q.; Srinivasan, V.; Balsara, N. P. Comparing Measurements of Limiting Current of Electrolytes with Theoretical Predictions up to the Solubility Limit. *J. Phys. Chem. C* **2019**, *123*, 23872–23881. https://doi.org/10.1021/acs.jpcc.9b07121.

(19) Laoire, C. O.; Plichta, E.; Hendrickson, M.; Mukerjee, S.; Abraham, K. M. Electrochemical Studies of Ferrocene in a Lithium Ion Conducting Organic Carbonate Electrolyte. *Electrochim. Acta* **2009**, *54* (26), 6560–6564. https://doi.org/10.1016/j.electacta.2009.06.041.

(20) Lee, S. I.; Jung, U. H.; Kim, Y. S.; Kim, M. H.; Ahn, D. J.; Chun, H. S. A Study of Electrochemical Kinetics of Lithium Ion in Organic Electrolytes. *Korean J. Chem. Eng.* **2002**, *19* (4), 638–644. https://doi.org/10.1007/BF02699310.

(21) Park, J. W.; Yoshida, K.; Tachikawa, N.; Dokko, K.; Watanabe, M. Limiting Current Density in Bis(Trifluoromethylsulfonyl)Amide-Based Ionic Liquid for Lithium Batteries. *J. Power Sources* **2011**, *196* (4), 2264–2268. https://doi.org/10.1016/j.jpowsour.2010.09.067.

(22) Hudson, W. R. Block Copolymer Electrolytes for Lithium Batteries, University of California, Berkeley, 2011.

(23) Gribble, D. A.; Frenck, L.; Shah, D. B.; Maslyn, J. A.; Loo, W. S.; Mongcopa, K. I. S.; Pesko, D. M.; Balsara, N. P. Comparing Experimental Measurements of Limiting Current in Polymer Electrolytes with Theoretical Predictions. *J. Electrochem. Soc.* **2019**, *166* (14), A3228–A3234. https://doi.org/10.1149/2.0391914jes.

(24) Loo, W. S.; Faraone, A.; Grundy, L. S.; Gao, K. W.; Balsara, N. P. Polymer Dynamics in Block Copolymer Electrolytes Detected by Neutron Spin Echo. *ACS Macro Lett.* **2020**, *9*, 639–645. https://doi.org/10.1021/acsmacrolett.0c00236.

(25) Newman, J.; Thomas-Alyea, K. E. *Electrochemical Systems*, 3rd ed.; John Wiley & Sons, Inc., 2004.

(26) Pesko, D. M.; Timachova, K.; Bhattacharya, R.; Smith, M. C.; Villaluenga, I.; Newman, J.; Balsara, N. P. Negative Transference Numbers in Poly(Ethylene Oxide)-Based Electrolytes. *J. Electrochem. Soc.* **2017**, *164* (11), E3569–E3575. https://doi.org/10.1149/2.0581711jes.

(27) Villaluenga, I.; Pesko, D. M.; Timachova, K.; Feng, Z.; Newman, J.; Srinivasan, V.; Balsara, N. P. Negative Stefan-Maxwell Diffusion Coefficients and Complete Electrochemical Transport Characterization of Homopolymer and Block Copolymer Electrolytes. *J. Electrochem. Soc.* **2018**, *165* (11), A2766–A2773. https://doi.org/10.1149/2.0641811jes.

(28) Sax, J.; Ottino, J. M. Modeling of Transport of Small Molecules in Polymer Blends : Application of Effective Medium Theory. *Polym. Eng. Sci.* **1983**, *23* (3), 165–176.

(29) Balsara, N. P.; Newman, J.; Storage, E.; Berkeley, L. Relationship between Steady-State Current in Symmetric Cells and Transference Number of Electrolytes Comprising Univalent and Multivalent Ions. **2015**, *162* (14), 2720–2722. https://doi.org/10.1149/2.0651514jes.

(30) Pesko, D. M.; Feng, Z.; Sawhney, S.; Newman, J.; Srinivasan, V.; Balsara, N. P. Comparing Cycling Characteristics of Symmetric Lithium-Polymer-Lithium Cells with Theoretical Predictions. *J. Electrochem. Soc.* **2018**, *165* (13), A3186–A3194. https://doi.org/10.1149/2.0921813jes.

(31) Quirk, R. P.; Kim, J.; Kausch, C.; Chun, M. Butyllithium-Initiated Anionic Synthesis of Well-Defined Poly(Styrene-Block-Ethylene Oxide) Block Copolymers with Potasium Salt Additives. *Polym. Int.* **1996**, *39* (1), 3–10. https://doi.org/10.1002/(SICI)1097-0126(199601)39:1<3::AID-PI436>3.0.CO;2-O.

(32) Hadjichristidis, N.; Pitsikalis, M.; Pispas, S.; Iatrou, H. Polymers with Complex Architecture by Living Anionic Polymerization. *Chem. Rev.* **2001**, *101* (12), 3747–3792. https://doi.org/10.1021/cr9901337.

(33) Singh, M.; Odusanya, O.; Wilmes, G. M.; Eitouni, H. B.; Gomez, E. D.; Patel, A. J.; Chen, V. L.; Park, M. J.; Fragouli, P.; Iatrou, H.; Hadjichristidis, N.; Cookson, D.; Balsara, N. P. Effect of Molecular Weight on the Mechanical and Electrical Properties of Block Copolymer Electrolytes. *Macromolecules* **2007**, *40* (13), 4578–4585. https://doi.org/10.1021/ma0629541.

(34) Maslyn, J. A.; Loo, W. S.; McEntush, K. D.; Oh, H. J.; Harry, K. J.; Parkinson, D. Y.; Balsara, N. P. Growth of Lithium Dendrites and Globules through a Solid Block Copolymer Electrolyte as a Function of Current Density. *J. Phys. Chem. C* **2018**, *122*, acs.jpcc.8b06355. https://doi.org/10.1021/acs.jpcc.8b06355.

(35) Loo, W. S.; Mongcopa, K. I.; Gribble, D. A.; Faraone, A. A.; Balsara, N. P. Investigating the Effect of Added Salt on the Chain Dimensions of Poly(Ethylene Oxide) through Small-Angle Neutron Scattering. *Macromolecules* **2019**, *52* (22), 8724–8732.

https://doi.org/10.1021/acs.macromol.9b01509.

(36) Yuan, R.; Teran, A. A.; Gurevitch, I.; Mullin, S. A.; Wanakule, N. S.; Balsara, N. P. Ionic Conductivity of Low Molecular Weight Block Copolymer Electrolytes. *Macromolecules* **2013**, *46* (3), 914–921. https://doi.org/10.1021/ma3024552.

(37) Harry, K. J.; Hallinan, D. T.; Parkinson, D. Y.; MacDowell, A. A.; Balsara, N. P. Detection of Subsurface Structures underneath Dendrites Formed on Cycled Lithium Metal Electrodes. *Nat. Mater.* **2014**, *13* (1), 69–73. https://doi.org/10.1038/nmat3793.

(38) Harry, K. J.; Liao, X.; Parkinson, D. Y.; Minor, A. M.; Balsara, N. P. Electrochemical Deposition and Stripping Behavior of Lithium Metal across a Rigid Block Copolymer Electrolyte Membrane. *J. Electrochem. Soc.* **2015**, *162* (14), A2699–A2706. https://doi.org/10.1149/2.0321514jes.

(39) Maslyn, J. A.; Frenck, L.; Loo, W. S.; Parkinson, D. Y.; Balsara, N. P. Extended Cycling through Rigid Block Copolymer Electrolytes Enabled by Reducing Impurities in Lithium Metal Electrodes. *ACS Appl. Energy Mater.* **2019**, acsaem.9b01685. https://doi.org/10.1021/acsaem.9b01685.

(40) Frenck, L.; Maslyn, J. A.; Loo, W. S.; Parkinson, D. Y.; Balsara, N. P. Impact of Salt Concentration on Nonuniform Lithium Electrodeposition through Rigid Block Copolymer Electrolytes. *ACS Appl. Mater. Interfaces* **2019**, *11*, 47878–47885. https://doi.org/10.1021/acsami.9b15606.

(41) Doyle, M.; Newman, J.; Gozdz, A. S.; Schmutz, C. N.; Tarascon, J.-M. Comparison of Modeling Predictions with Experimental Data from Plastic Lithium Ion Cells. *J. Electrochem. Soc.* **1996**, *143* (6), 1890–1903. https://doi.org/10.1149/1.1836921.

(42) Pesko, D. M. Complete Electrochemical Characterization of Ion Transport in Polymer Electrolytes, p 128-130, 2018.

(43) Newman, J.; Chapman, T. W. Restricted Diffusion in Binary Solutions. *AIChE J.* **1973**, *19* (2), 343–348. https://doi.org/10.1002/aic.690190220.

(44) Thompson, S. D.; Newman, J. Differential Diffusion Coefficients of Sodium Polysulfide Melts. *J. Electrochem. Soc.* **1989**, *136* (11), 3362. https://doi.org/10.1149/1.2096451.

(45) Pandolfi, R. J.; Allan, D. B.; Arenholz, E.; Barroso-Luque, L.; Campbell, S. I.; Caswell, T. A.; Blair, A.; De Carlo, F.; Fackler, S.; Fournier, A. P.; Freychet, G.; Fukuto, M.; Gursoy, D.; Jiang, Z.; Krishnan, H.; Kumar, D.; Kline, R. J.; Li, R.; Liman, C.; Marchesini, S.; Ren, F.; Sahoo, S.; Strzalka, J.; Sunday, D.; Tassone, C. J.; Ushizima, D.; Venkatakrishnan, S.; Yager, K. G.; Zwart, P.; Sethian, J. A.; Hexemer, A. Xi-Cam: A Versatile Interface for Data Visualization and Analysis. *J. Appl. Synchrotron Radiat.* **2018**, *25*, 1261–1270.

(46) Monroe, C.; Newman, J. Dendrite Growth in Lithium/Polymer Systems. *J. Electrochem. Soc.* **2003**, *150* (10), A1377. https://doi.org/10.1149/1.1606686.

(47) Newman, J.; Balsara, N. P. *Electrochemical Systems*, 4th ed.; Wiley, 2021.

(48) Sharon, D.; Bennington, P.; Dolejsi, M.; Webb, M. A.; Dong, X.; de Pablo, J. J.; Nealey, P. F.; Patel, S. N. Intrinsic Ion Transport Properties of Block Copolymer Electrolytes. *ACS Nano* **2020**. https://doi.org/10.1021/acsnano.0c03713.

(49) Galluzzo, M. D.; Loo, W. S.; Wang, A. A.; Walton, A.; Maslyn, J. A.; Balsara, N. P. Measurement of Three Transport Coefficients and the Thermodynamic Factor in Block Copolymer Electrolytes with Different Morphologies. *J. Phys. Chem. B* **2020**, *124* (5), 921–935. https://doi.org/10.1021/acs.jpcb.9b11066.

(50) Frenck, L.; Veeraraghavan, V. D.; Maslyn, J. A.; Müller, A.; Ho, A. S.; Loo, W. S.; Minor, A. M.; Balsara, N. P. Effect of Salt Concentration Profiles on Protrusion Growth in Lithium-Polymer-lithium Cells. *Solid State Ionics* **2020**, *358*, 115517. https://doi.org/10.1016/j.ssi.2020.115517.